Electronic Supplementary Material (ESI) for RSC Advances.

Supporting Information

Mixed metallic node effect in zeolitic imidazolate frameworks

Table S1. Densities (g/cm^3) of Zn-ZIF-62 from experiments and density functional theory (DFT) and classical force field (FF) calculations. The solvent content was taken from the literature[1] and added to the density calculation for the DFT and FF results.

	Zn-ZIF-62 crystal
Exp.[1]	1.494
Current Exp.	1.467
DFT (PBE-D3)	1.537
FF	1.546

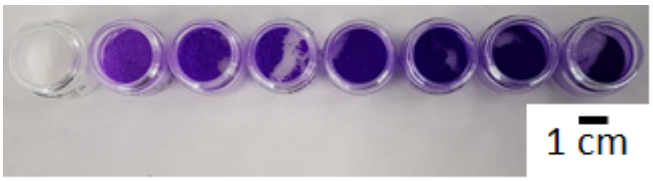

Fig. S1. Image of Co/Zn-ZIF-62 samples (from the left 0.0, 0.1, 0.2, 0.4, 0.6, 0.8, 0.9, 1.0) revealing the change in the intensity of the purple colour with increasing cobalt content.

UV-VIS Absorption analysis of Co/Zn-ZIF-62

UV-VIS was carried out to verify that the intensity of purple colour of the bimetallic ZIF-62 crystals correlates with the cobalt content. Calibration curve was used by dissolving 0.0482 grams of 1.0-ZIF-62 using 10 mL 1 M HCl. The solution was used for a full UV-VIS absorption spectrum using a Varian Cary 50 Bio UV-Visible Spectrophotometer. The result showed a peak absorption at 510 nm (green), which has red as its complimentary colour. The solution was then diluted, using 1 M HCl with the following solution:HCl ratios: 9:1, 8:2, 7:3, and 6:4. The samples were then measured on a thermo spectronic helios epsilon spectrophotometer at 510 nm to measure the absorption. The data was used to make a calibration curve, using a linear fit with $R^2 = 0.999$. For each Co and Zn-containing ZIF-62 sample, a weighed amount was dissolved, using 1 M HCl and their absorption were measured at 510 nm. A theoretical absorption for a pure Co-ZIF-62 was calculated for each sample to reveal the [Co]/[Co+Zn] rat io.Fig S2. displays the observed relative Co content against the

fraction of Co used in the synthesis. The figure displays a fairly good agreement between synthesis condition and the content of cobalt in the sample.

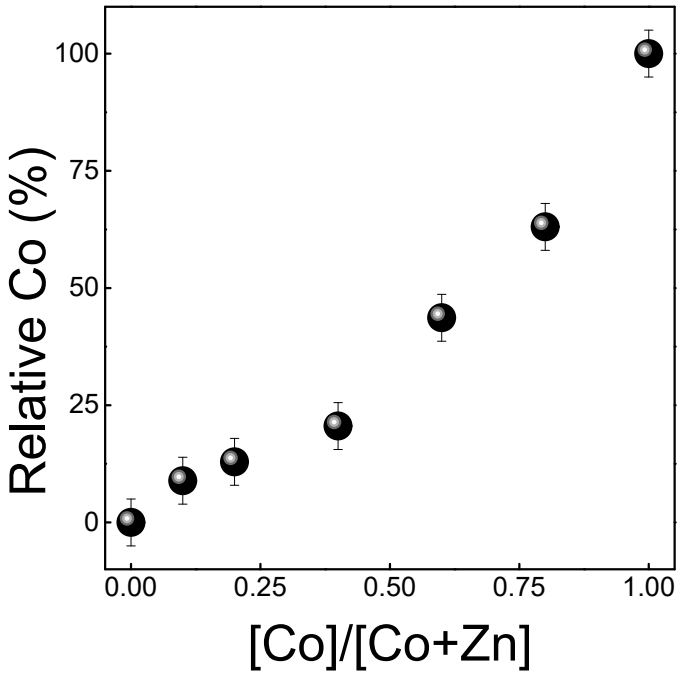

Fig S2. Observed cobalt content plotted against the ratio used during synthesis of Co/Zn-ZIF-62.

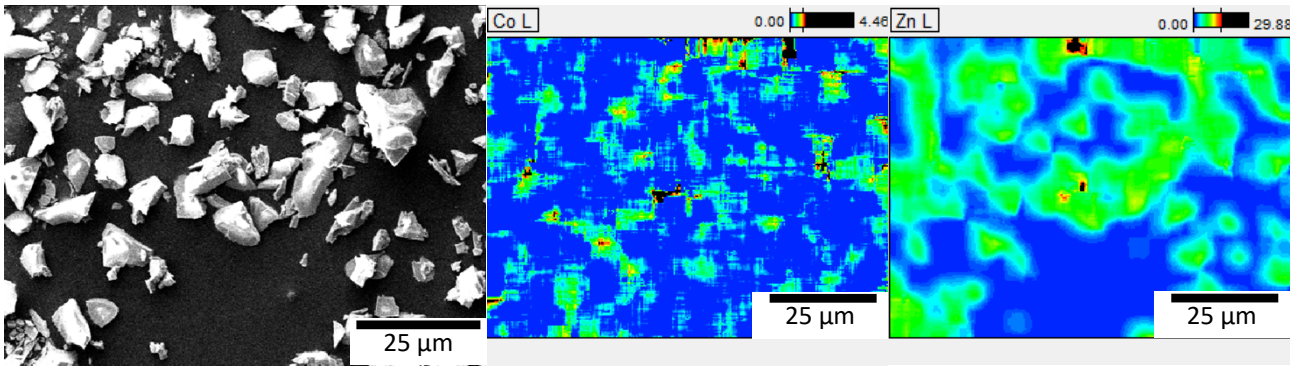

Fig S3. SEM image (left) of the area detected by EDX for 0.0-ZIF-62 sample, and the EDX elemental mapping for the cobalt (middle column) and zinc (right column), using a contoured color gradient.

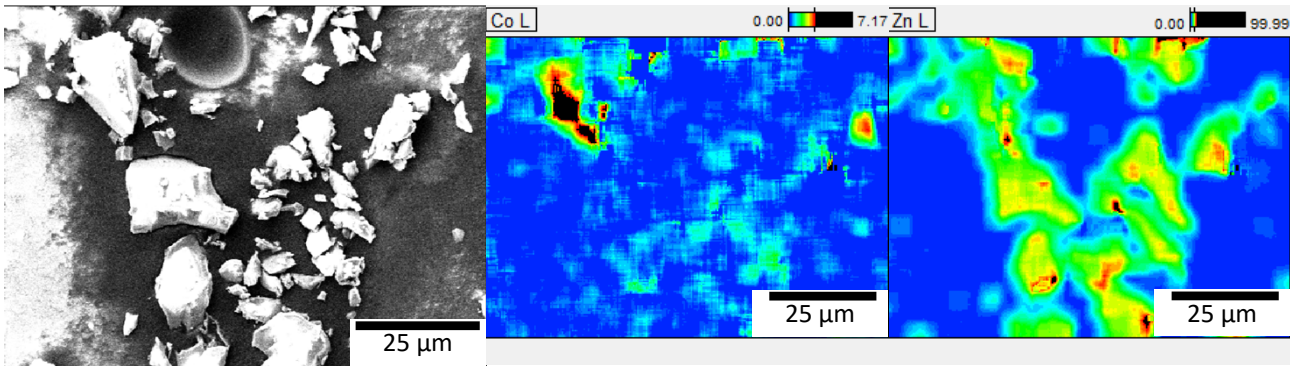

Fig. S4. SEM image (left) of the area detected by EDX for 0.1-ZIF-62 sample, and the EDX elemental mapping for the cobalt (middle column) and zinc (right column), using a contoured color gradient.

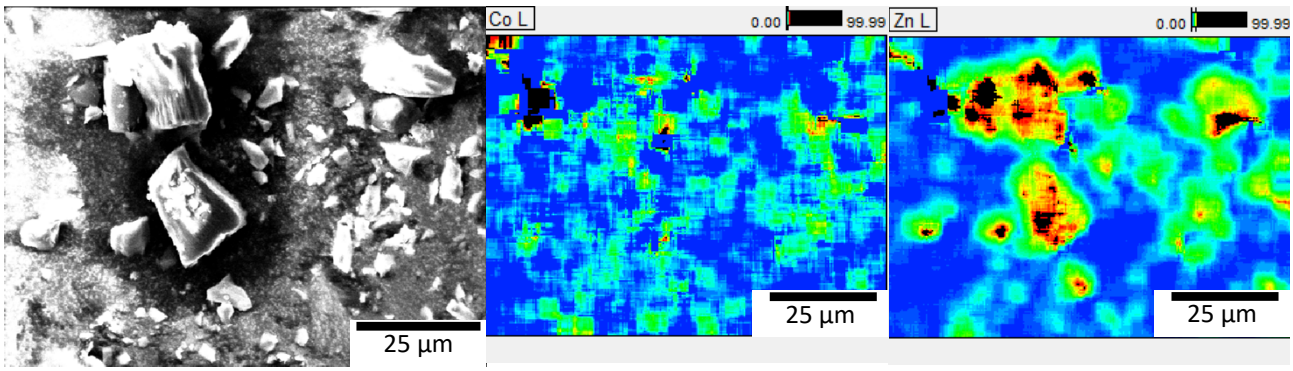

Fig. S5. SEM image (left) of the area detected by EDX for 0.2-ZIF-62 sample, and the EDX elemental mapping for the cobalt (middle column) and zinc (right column), using a contoured color gradient.

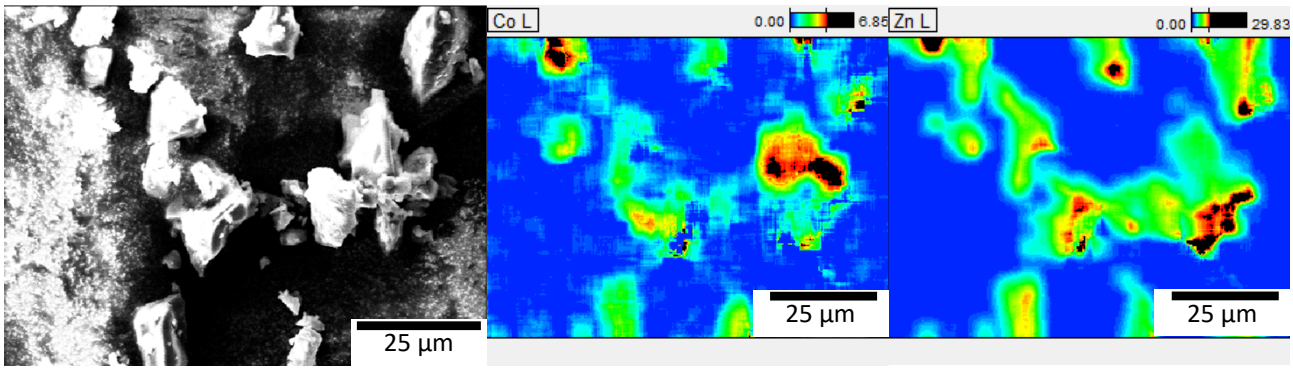

Fig. S6. SEM image (left) of the area detected by EDX for 0.4-ZIF-62 sample, and the EDX elemental mapping for the cobalt (middle column) and zinc (right column), using a contoured color gradient.

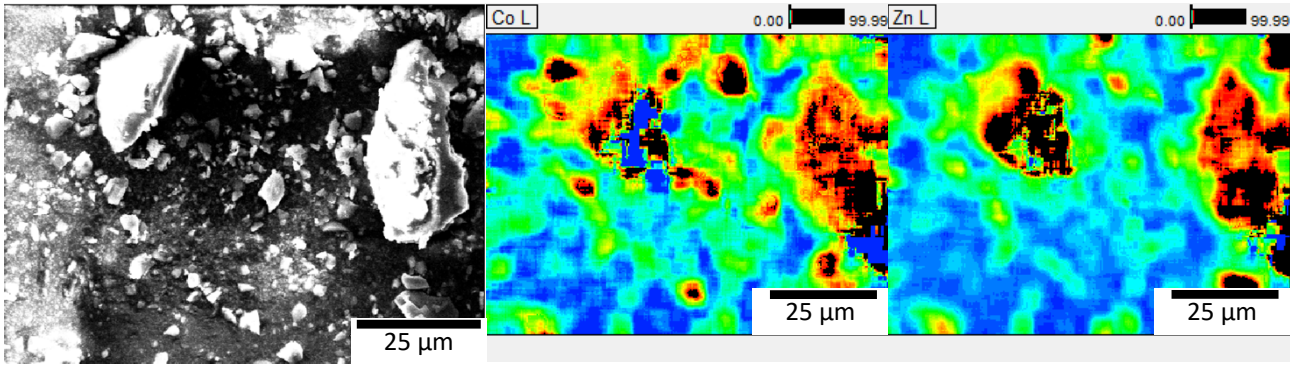

Fig. S7. SEM image (left) of the area detected by EDX for 0.6-ZIF-62 sample, and the EDX elemental mapping for the cobalt (middle column) and zinc (right column), using a contoured color gradient.

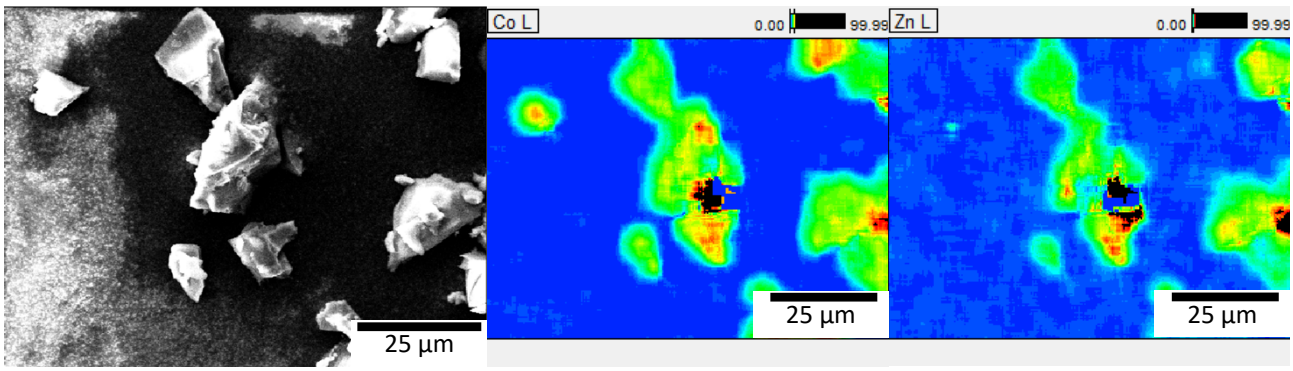

Fig. S8. SEM image (left) of the area detected by EDX for 0.8-ZIF-62 sample, and the EDX elemental mapping for the cobalt (middle column) and zinc (right column), using a contoured color gradient.

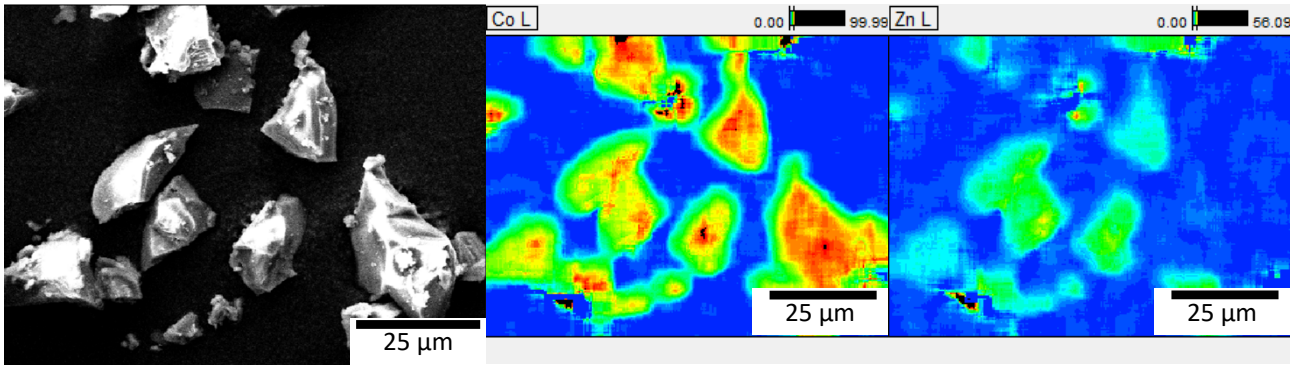

Fig. S9. SEM image (left) of the area detected by EDX for 0.9-ZIF-62 sample, and the EDX elemental mapping for the cobalt (middle column) and zinc (right column), using a contoured color gradient.

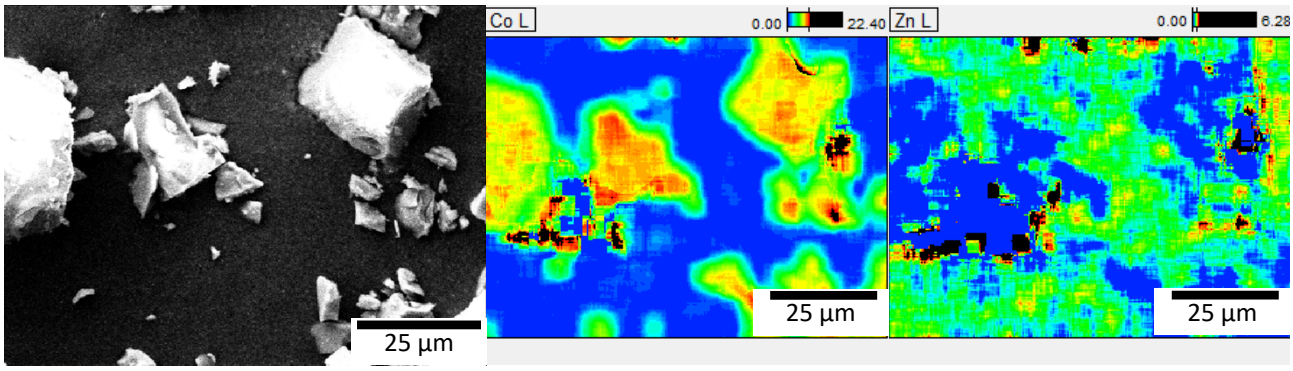

Fig. S10. SEM image (left) of the area detected by EDX for 1.0-ZIF-62 sample, and the EDX elemental mapping for the cobalt (middle column) and zinc (right column), using a contoured color gradient.

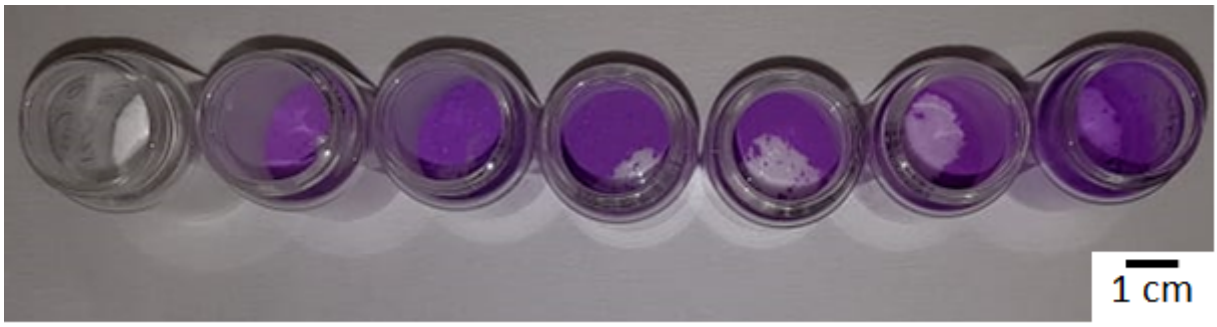

Fig. S11. Image of Co/Zn-ZIF-new samples (from the left 0.0, 0.1, 0.2, 0.4, 0.6, 0.8, 1.0), revealing the change in the intensity of the purple colour with increasing cobalt content.

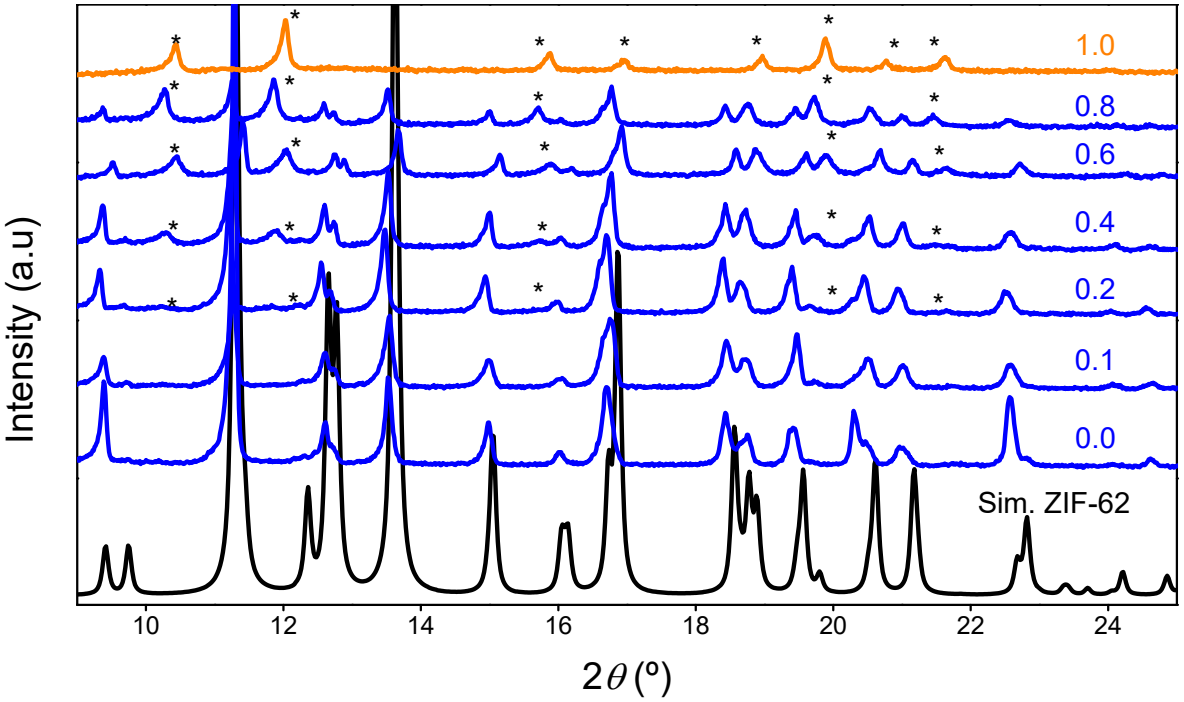

Fig. S12. X-ray diffraction patterns of Co/Zn-ZIF-new, showing the emergence of a new crystalline phase, as Co substitutes for Zn. Emerging new peaks are designated with *.

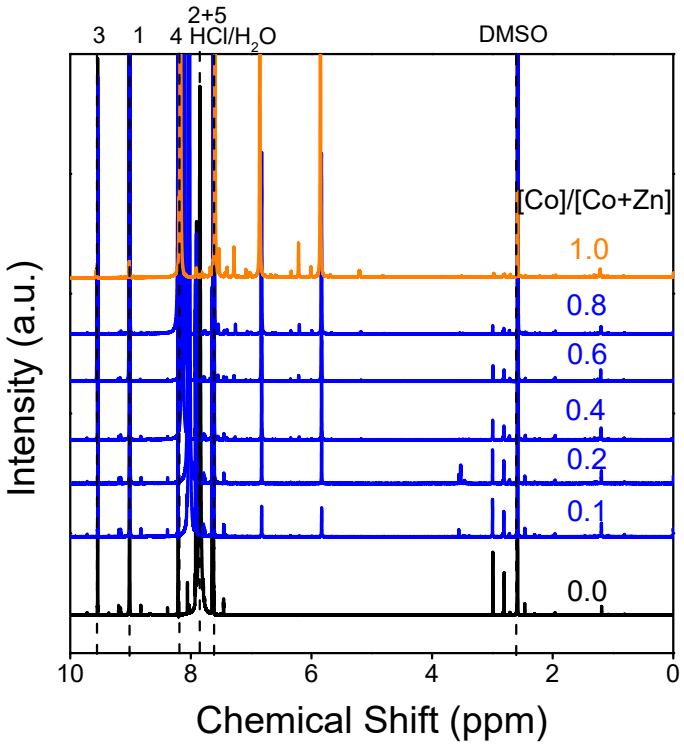

Fig. S13. Liquid ^{1}H-NMR spectra of Co/Zn-ZIF-new samples. The emergence of two new peaks as cobalt substitutes for zinc reveals the formation of a new organic linker during the synthesis.

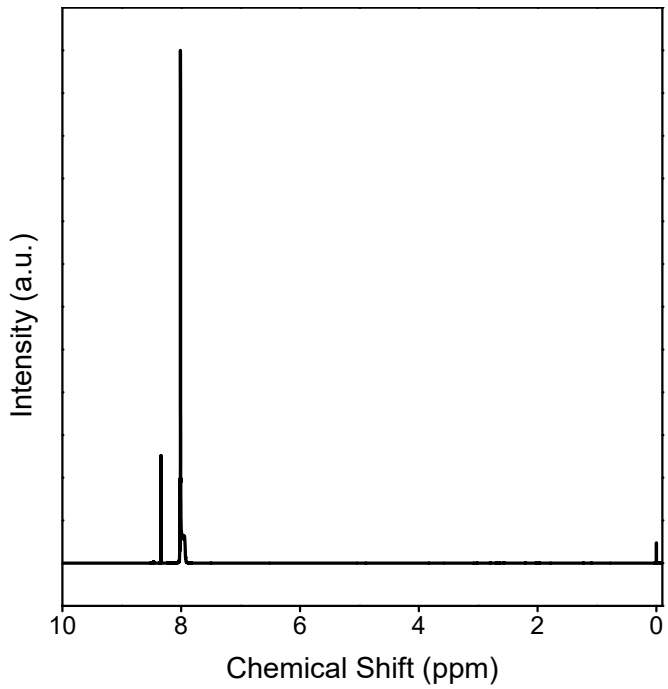

Fig. S14. Liquid ^{1}H-NMR spectrum of 4-nitroimidazole purchased from Sigma Aldrich (97%).

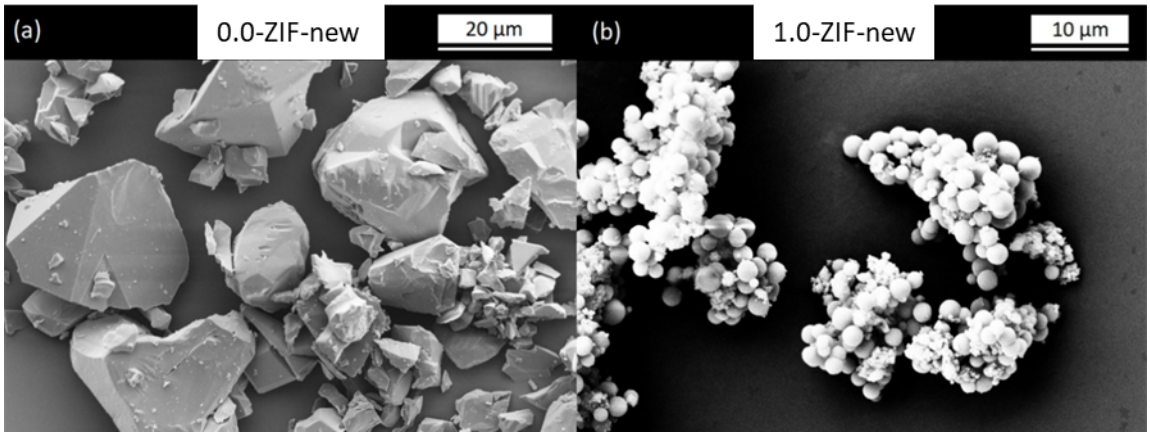

Fig. S15. SEM images of crystalline ZIF-new samples. (a) 0.0-ZIF-new. (b) 1.0-ZIF-new

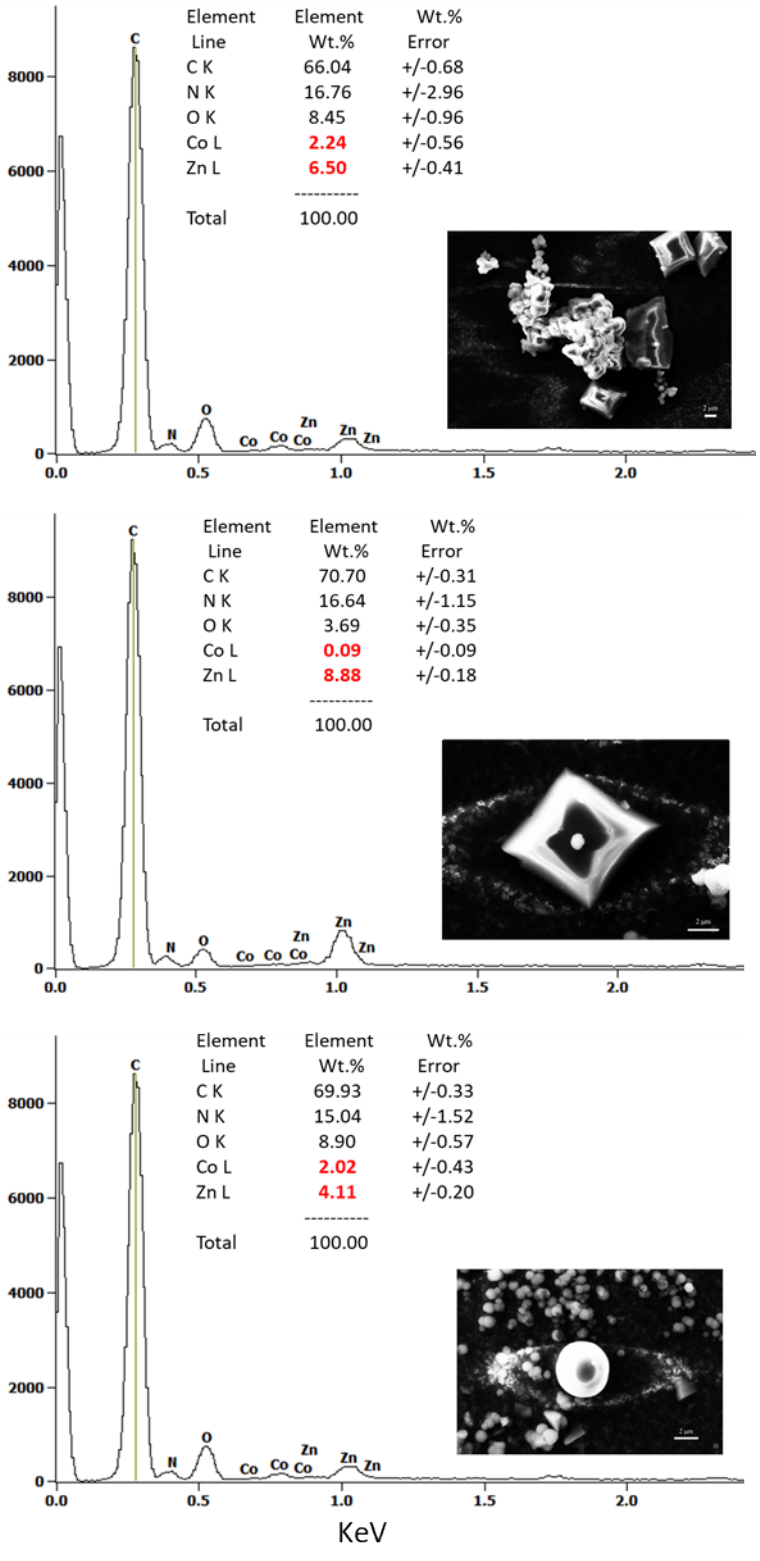

Fig. S16. EDX elemental analysis of different particles belonging to the 0.6-ZIF-new sample, showing chemical heterogeneity in the sample.

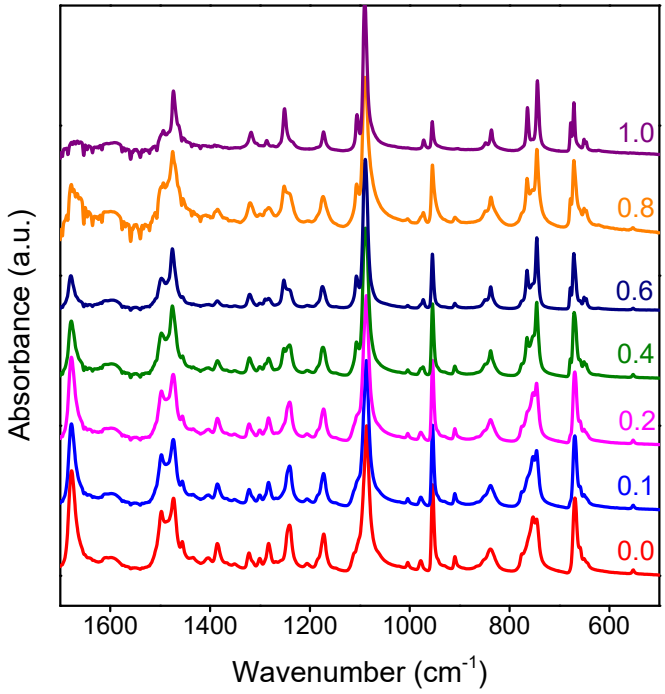

Figure S17. ATR FT-IR spectrum of Co/Zn-ZIF-new samples.

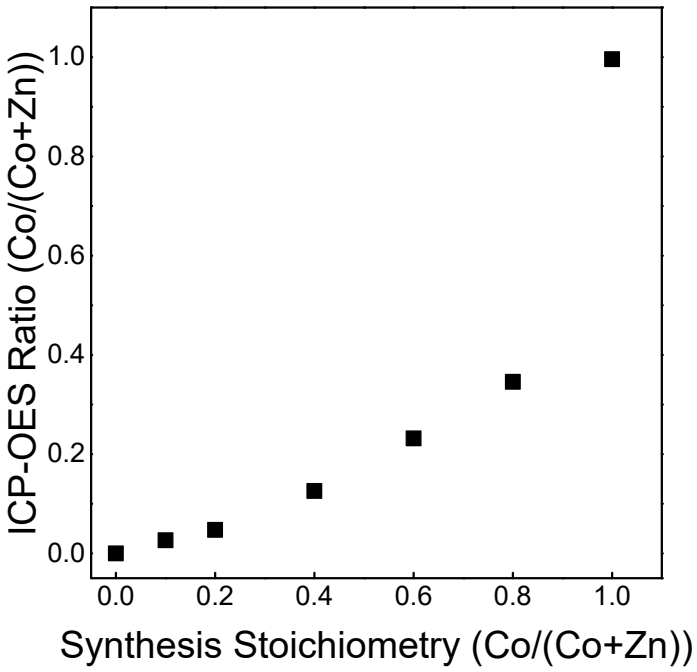

Fig. S18. Measured Co/(Co+Zn) ratio vs. synthesis stoichiometry for Co/Zn-ZIF-new samples. Inductively coupled plasma – optical emission spectroscopy (ICP-OES) (Prodigy 7, Teledyne Leeman Labs) analysis was used to quantify the zinc to cobalt ratio. The standard calibration solutions used

contains 1 µg mL^{-1} Zn, Ni Cr and 0.5 µg mL^{-1} Ba, Mn, Cu in 3% HNO_3 (National Institute of Metrology, China). Sample solutions were prepared by dissolving a precisely weighed amount of ZIF sample into 2 mL of an HNO_3 solution. The primary solutions were transferred to 50 mL volumetric flasks readied for measurements. For quantitative analysis of Zn and Co, the wavelengths 206.200 nm and 228.615 nm were used, respectively.

Fig. S19. Image of 0.4-ZIF-new, revealing a rich purple phase and a lighter phase being separated during the drying process.

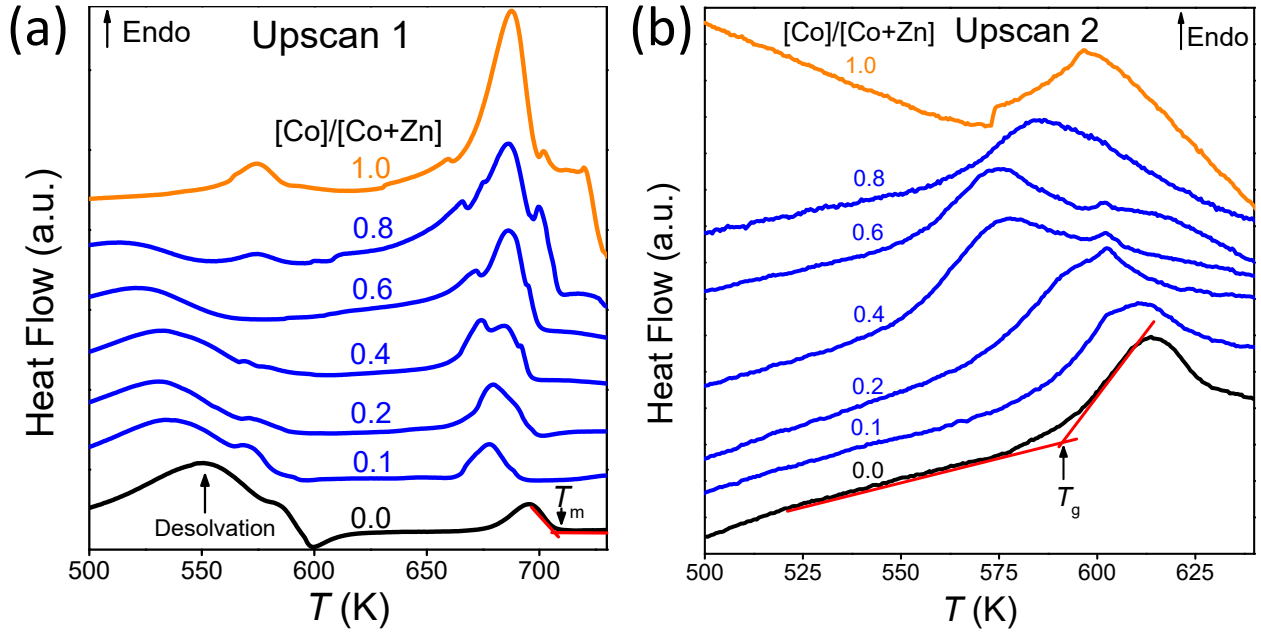

Fig. S20. DSC analysis of Co/Zn-ZIF-new. (a) first upscan (heating rate of 10 K min^{-1}) revealing the endothermic solvent release and melting point and partial decomposition. (b) second upscan (10 K min^{-1}) revealing the glass transition peak onset.

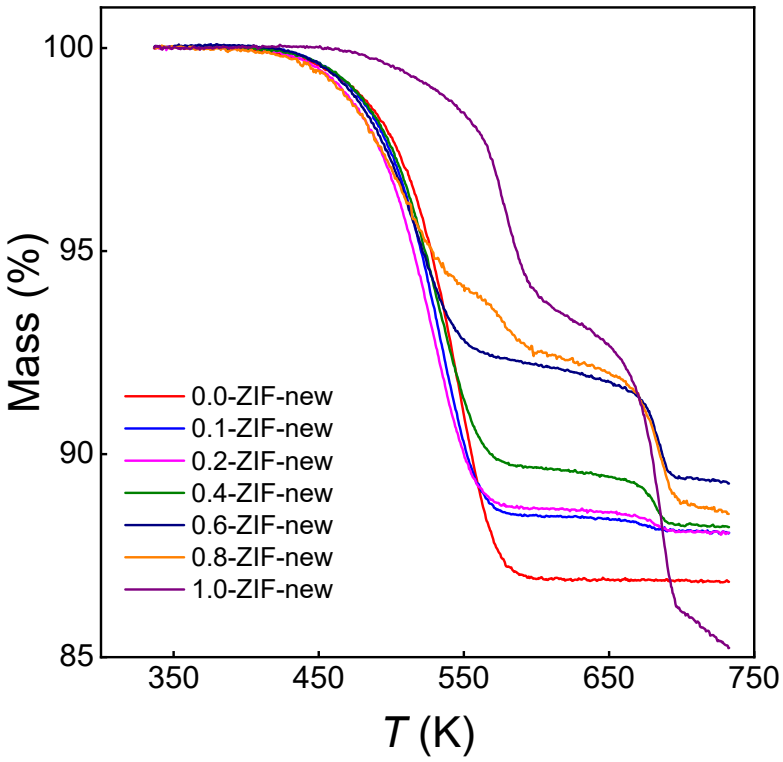

Figure S21. TGA data of synthesized Co/Zn-ZIF-new crystals during the first upscan.

Biphasic Decomposition Gas Analysis

Thermal gravimetric analyses (TGA) were performed using a Jupiter 449 simultaneous thermal analysis instrument (Netzch, Selb, Germany) coupled with a 403C Aëoloss mass spectrometer (MS), with a heating rate of 10 °C min^{-1} in an argon atmosphere. The ionized species of the gases released from the heat-treated sample were detected by the MS. The MS data were compared to the gas ionic spectra of the relevant gases from the NIST Standard Reference Database[1]. The gases we identified based on the m/z numbers and their relative intensity. The signals from MS are not quantitative.

The mass loss for the sample 0.0-ZIF-new is related to the release of N_2 and/or CO (m/z=28), H_2O (m/z=18), NO (m/z=30), DMF (m/z=73, 44, 42, 29), and NH_3 (m/z=17, 16). The ionic spectra for the first mass loss of the sample 1.0-ZIF-new indicate release of H_2O, N_2 and/or CO, NO, and NH_3, while the spectra for the second mass at >370 °C indicate release of NH_3, NO, and small amounts of CH_4 (m/z=15) and CO_2. These data show that the organic constituents (e.g., DMF) in great part degrade to smaller molecules (e.g., N_2, NO, NH_3) when leaving the analyzed sample.

[1] P.J. Linstrom and W.G. Mallard, Eds., NIST Chemistry WebBook, NIST Standard Reference Database Number 69, National Institute of Standards and Technology 2005, Gaithersburg MD, 20899, http://webbook.nist.gov, (accessed 30.8.2021)

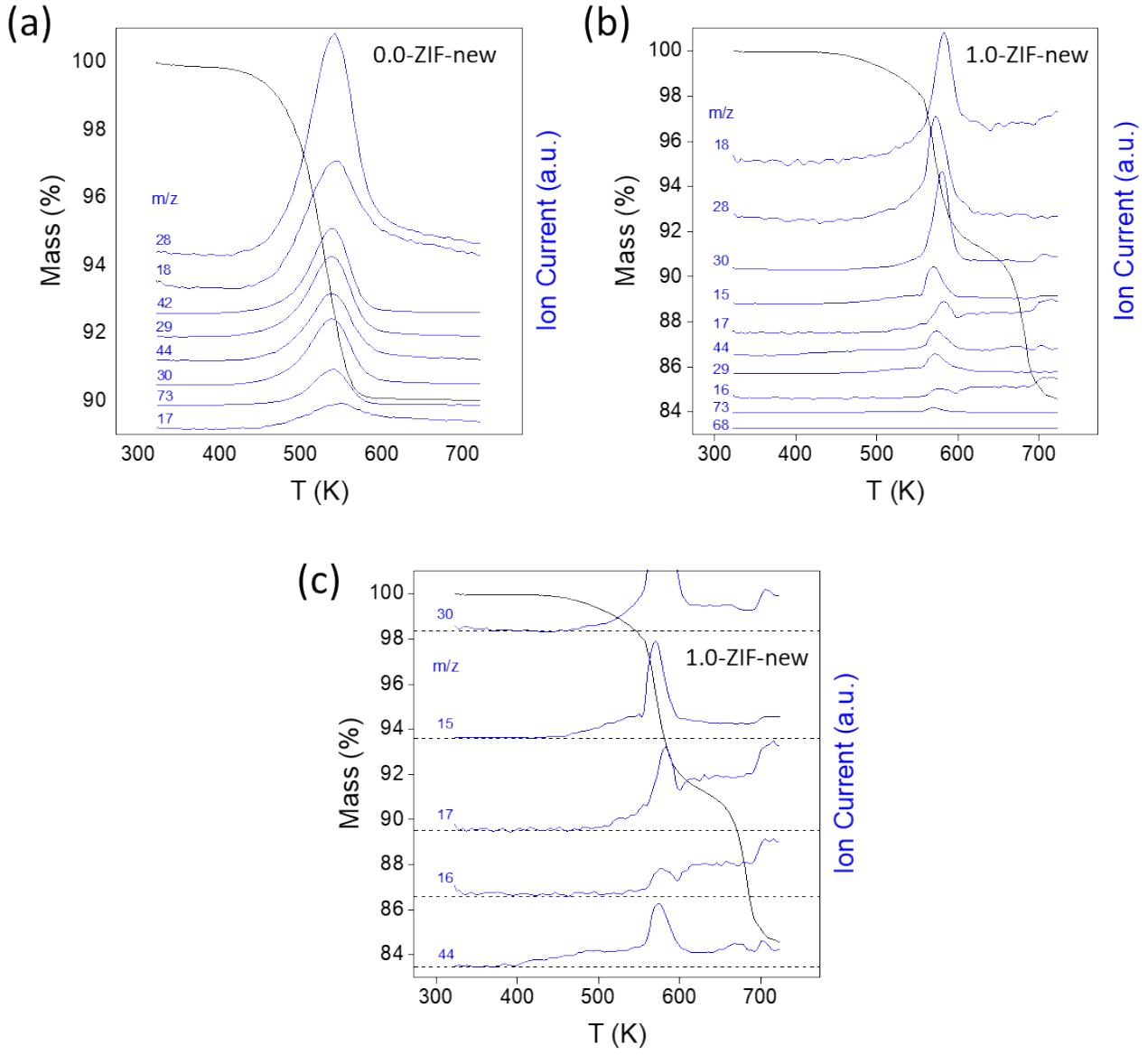

Fig. S22. DTA-MS spectra of the samples (a) 0.0-ZIF-new and (b,c) sample 1.0-ZIF-new. (c) focuses on the second mass at >370 °C and shows the ionic signals of the gases that remain high above their baselines (thin dotted lines).

References

1 T. D. Bennett, Y. Yue, P. Li, A. Qiao, H. Tao, N. G. Greaves, T. Richards, G. I. Lampronti, S. A. T. Redfern, F. Blanc, O. K. Farha, J. T. Hupp, A. K. Cheetham and D. A. Keen, J. Am. Chem. Soc., 2016, **138**, 3484–3492.

2 L. Frentzel-Beyme, M. Kloß, R. Pallach, S. Salamon, H. Moldenhauer, J. Landers, H. Wende, J. Debus and S. Henke, J. Mater. Chem. A, 2019, **7**, 985–990.